FEATURE ARTICLE

Growth of Oxide Nanorod Arrays through Sol Electrophoretic Deposition

Guozhong Cao*

Department of Materials Science and Engineering, University of Washington, Seattle, Washington 98195

Received: July 16, 2004

This article introduces a process for the growth of oxide nanorod arrays that combines sol preparation and template-based electrophoretic deposition. First, fundamentals and practical approaches in sol−gel processing for synthesis of inorganic or inorganic/organic hybrid materials are briefly described. Second, electrophoresis in colloidal dispersions and electrophoretic deposition technique are discussed. Particular attention is devoted to the electrophoretic deposition for the growth of oxide nanorod arrays from sols. Finally, techniques similar to or derived from sol electrophoretic deposition for the growth of single crystalline oxide nanorod arrays are presented with vanadium pentoxide as a model system. Further examples are shown that the sol electrophoretic deposition is an effective method for the formation of conformal coating of thin films of oxides on metal nanorods to produce metal-oxide core−shell nanocable arrays. Relations between processing conditions, growth parameters, morphologies, microstructures, and properties of nanorod arrays are reviewed.

1. Introduction

Metal oxides, particularly complex metal oxides, are important materials for various applications in industry and technology. This is due to their multi-faceted functional properties, their chemical and thermal stability, and their mechanical properties. Metal oxides (and particularly complex metal oxides) can have many unique physical properties including electronic and ionic conductivity, superconductivity, ferroelectricity, piezoelectricity, dielectric, electrooptic, electrochemical, and magnetic properties.[1] These materials find a wide range of applications in electronic devices, sensors, and actuators. For example, piezoelectrics (typically lead zirconate titanate, PZT) play a key role in many micro electro-mechanical systems (MEMS).[2] Tin doped indium oxide (ITO) films on glass substrates have been widely used as optically transparent electrodes in devices such as light-emitting diodes.[3] Intercalation oxides, such as RuO_2 and V_2O_5, are extensively studied for electrochemical pseudocapacitor applications.[4] Sol−gel derived mesoporous titania films are being intensively studied in inorganic−organic hybrid photoelectrochemical cells.[5] Further, many of the physical properties of oxide materials are tunable through appropriate doping or substitution.[6] Zirconia that is partially stabilized through doping with materials such as calcium oxide or yttrium oxide exhibits excellent mechanical properties, particularly toughness not commonly found in other oxide materials.[7] Doped zirconia is also an excellent oxygen ionic conductor, with applications in oxygen sensors and solid oxide fuel cells (SOFC).[7] Oxide surfaces can have special chemical properties, making them useful as catalysts and sensors.[8] Furthermore, oxide surfaces can be easily incorporated with organic functional groups through surface condensation or self-assembly.[9]

For many applications of metal oxides as mentioned above, the sensitivity or efficiency obtained is directly proportional to the surface area of the material. Nanorods or nanowires can offer a significantly larger surface area than that of films or the bulk material. Although nanorods or nanowires have smaller surface area as compared with nanoparticles, they offer a great advantage in device fabrication. Uniformly sized nanorods or nanowires with unidirectional alignment are particularly useful and are referred to as nanorod arrays hereinafter. Nanorods or nanowires can function as both structural and functional components in devices. Further, nanorods and nanowires can offer various physical properties, and thus find diverse applications in nanotechnology. Nanorods or nanowires also provide the opportunity to study the physical properties of one-dimensional structures.

Numerous researchers have studied the synthesis and fabrication of oxide nanorods and nanowires, and many different synthesis techniques have been developed.[10] Elegant single crystal oxide nanowires and nanobelts can grow directly through evaporation−condensation process at elevated temperatures under moderate vacuum.[11] Growth of oxide nanorod arrays requires extra control of growth direction as well as size of nanorods. Examples include oxidation of metallic nanorods, vapor−liquid−solid (VLS) growth under vacuum, seeded growth, and template filling of oxide colloidal particles. Oxidation of metallic nanorods or nanowires is one established method to create oxide nanorods. However, this method is likely to be limited to simple metal oxide nanorods.[12] VLS growth of oxide nanorods and nanowires is restricted to systems that can form a eutectic liquid with catalyst at growth temperature.[13] There is very limited information in the literature about the formation of eutectic liquids in complex oxide and catalyst systems. Further, compared to other materials, oxides typically possess a high melting point and are thus likely to form a eutectic liquid only at high temperatures, requiring a high

* To whom correspondence should be addressed. E-mail: gzcao@u.washington.edu.

10.1021/jp040492s CCC: $27.50
Published on Web 11/24/2004

processing temperature for the growth of nanorods. Seeded growth is another method to synthesize oxide nanorod arrays.[14,15] It is practically a very useful technique in growing single crystal oxide nanorod arrays for many applications; however, this method suffers from the fact that grown nanorods usually possess an inverse conical shape if care is not taken, starting with a smaller diameter at the bottom and progressively becoming larger and larger as growth proceeds.

Martin and co-workers,[16] along with a few other groups, have published extensively on the fabrication of oxide nanorod arrays by filling templates with sols or colloid dispersions. Many oxide nanorods have been synthesized with this method. Examples include nanorods of TiO_2, V_2O_5, WO_3, ZnO,[16] Ga_2O_3, and In_2O_3.[17] This method does offer several advantages over the VLS technique, seeded growth, and oxidation of metallic nanorods or nanowires, though template dependent. One of the advantages is the possibility of fabrication of complex oxide nanorods with precise control of stoichiometric composition. Another advantage is the simplicity of the method. Further, it offers the possibility to fabricate unidirectionally aligned and uniformly sized oxide nanorods over a large area, which is particularly attractive for device fabrication and property characterization. However, complete filling of solid inside holes could be challenging, considering the fact that typical sols or colloidal dispersions consist of 10% or less solid dispersed in a solvent. In fact, hollow tubes are often obtained from this technique instead of solid rods.[16,17] In this article, we summarize an approach to synthesis and fabrication of nanorod arrays of oxides with template-based sol electrophoretic deposition (EPD). This approach combines several processing methods together: including sol−gel processing, electrophoretic deposition, and template-based growth. This method offers the possibility of making nanorod arrays of oxides, organic−inorganic hybrids and bio-inorganic hybrids.

2. Sol−Gel Processing

Sol−gel processing is a wet chemical route for the synthesis and processing of inorganic and organic−inorganic hybrid materials. Sol−gel processing offers many advantages, including low processing temperature (typically <100 °C) and molecular level homogeneity. Sol−gel processing is particularly useful in making complex metal oxides and temperature sensitive organic−inorganic hybrid materials. This section will briefly summarize some fundamentals and key issues of sol−gel processing. For more details, readers may wish to consult the abundant literature in this field. For instance, the books *Sol−Gel Science* by Brinker and Scherer,[18] *Introduction to Sol−Gel Processing* by Pierre,[19] and *Sol−Gel Materials* by Wright and Sommerdijk[20] provide excellent comprehensive coverage on sol−gel processing and materials.

Typical sol−gel processing consists of hydrolysis and condensation of precursors. Precursors can be either organic, such as metal alkoxides, or inorganic salts. Organic or aqueous solvents may be used to dissolve precursors, and catalysts are often added to promote and/or control both hydrolysis and condensation reactions

$$M(OEt)_4 + xH_2O \rightarrow M(OEt)_{4-x}(OH)_x + xEtOH \quad (1)$$

$$M(OEt)_{4-x}(OH)_x + M(OEt)_{4-x}(OH)_x \rightarrow (OEt)_{4-x}(OH)_{x-1}M-O-M(OEt)_{4-x}(OH)_{x-1} + H_2O \quad (2)$$

Hydrolysis (reaction 1) and condensation (reaction 2) are both multiple-step processes, occurring sequentially and in parallel. Condensation results in the formation of nanoscale clusters of metal oxides and hydroxides, often with organic groups attached to them. These organic groups may be due to incomplete hydrolysis or introduced as non-hydrolyzable organic ligands. The size of the nanoscale clusters, along with the morphology and microstructure of the final product, can be tailored by controlling the hydrolysis and condensation reactions.

One of the greatest advantages of sol−gel processing is the ability to synthesize and process complex oxides. This requires appropriate design and control of the hydrolysis and condensation reactions of the various constituent precursors. Ideally, the constituent materials should be homogeneously mixed at the atomic/molecular level, with the desired stoichiometric ratio in each nanoscale clusters. The challenge comes from the fact that each precursor can have different chemical reactivity, so that the hydrolysis and condensation reaction rates may differ significantly from one to another. Consequently, each precursor may form nanoclusters of its own (single) metal oxide, yielding a mixture of nanoscale particles of constituent simple oxides in the sol. The resulting product would be a mixture or a composite of multiple oxide phases, instead of a single-phase complex oxide.

There are several ways to avoid this homo-condensation and achieve a homogeneous mixture of multiple components at the molecular/atomic level. Modification of precursors, the use of complex precursors, partial hydrolysis and multistep hydrolysis, and condensation are the common approaches. Another problem in making complex oxide sols is that the constituent precursors may exert a catalytic effect on one another. As a result, the hydrolysis and condensation reaction rates in combination may be significantly different from those when the precursors are processed separately.

Incorporating organic components into an oxide system by sol−gel processing makes it easy to form organic−inorganic hybrids. One approach is to copolymerize or co-condense both the inorganic precursor(s), which leads to the formation of the inorganic component, and the organic precursor(s), which consists of non-hydrolyzable organic groups. Such organic−inorganic hybrids are a single-phase material, in which the organic and inorganic components are linked through chemical bonds. Another approach is to trap the desired organic components physically inside the inorganic or oxide network, by either homogeneously dispersing the organic components in the sol, or infiltrating the organic molecules into the gel network. Similar approaches can be applied for the incorporation of bio-components into oxide systems. Another method to incorporate bio-components into the oxide structure is to use functional organic groups to bridge inorganic and biological species.

In sol preparation, limited attention has been paid to the control of crystallization or formation of crystal structure, although the formation of crystalline structure without high-temperature firing is desired for some applications. Matsuda and co-workers have demonstrated that it is possible to form the crystalline phase of $BaTiO_3$ without high temperature sintering by carefully controlling processing conditions, including concentrations and temperature.[21]

By a careful control of sol preparation and processing, monodisperse nanoscale particles of various oxides, including complex oxides, organic−inorganic hybrids and biomaterials, can be synthesized. The key issue is to promote a simultaneous homogeneous nucleation, followed with a diffusion-controlled growth.[10,22,23] The particle size can be varied by changing the concentration and aging time.[18] In a typical sol, nanoclusters formed by hydrolysis and condensation reactions commonly

have a size ranging from 1 to 100 nm. Such nanoparticles have many applications in nanostructured material fabrication and processing. For example, they are building blocks for the formation of photonic band gap crystals.[24] Other researchers have explored the use of these nanoscale particles for optical applications by constructing various core−shell structures.[25]

In a sol, just like in other colloidal systems, gravity is a negligible factor, whereas Brownian motion plays an important role. Nanoclusters or nanoparticles possess a huge surface area/volume ratio and thus a large surface energy. There is a strong tendency for such nanoscale clusters to agglomerate. Two types of mechanisms are available to prevent such agglomeration in a sol. One is polymeric or steric stabilization, and the other is electrostatic stabilization. Polymeric stabilization works by adsorbing polymeric molecules onto the nanocluster or nanoparticle surface; spatial exclusion then prevents two clusters from getting close enough to agglomerate. Electrostatic stabilization is based on the surface charge of nanoclusters or nanoparticles in a sol. Such a surface charge will interact with other charged species in the sol to form a charged structure around the particle, which in turn introduces an energy barrier to prevent two particles from approaching one another. Electrosteric stabilization is another mechanism, which combines steric and electrostatic stabilization mechanisms, where the electrostatic effect is due either to the surface charge on the solid surface, or an uneven charge distribution in the polymer molecules.

A sol is a very dilute system, typically consisting of 90% or more solvent by volume. Upon drying, there can be a significant amount of shrinkage, resulting in severe cracking in sol−gel derived films and monoliths. The formation of cracks often limits sol−gel processing to the synthesis of thin films and structures less than a micron in size. This limitation, however, would not be a problem for the fabrication and process of nanostructured materials. Another potential limitation for some applications is that sol−gel-derived films or monoliths are highly porous. A sintering process at elevated temperatures is often required to obtain dense films or monoliths. Furthermore, sol−gel processing often produces amorphous oxides, potentially requiring elevated temperatures for crystallization.

3. Electrophoretic Deposition

The electrophoretic deposition (EPD) technique has been widely explored, particularly in film deposition from colloidal dispersions. As briefly mentioned in the previous section, nanosized particles in colloidal dispersions including sols can be stabilized by electrostatic or electrosteric mechanisms. When dispersed in a polar solvent or an electrolyte solution, the surface of nanoparticles develops an electrical charge via one or more of the following mechanisms: (1) preferential dissolution or (2) deposition of charges or charged species, (3) preferential reduction or (4) oxidation, and (5) adsorption of charged species such as polymers. Charged surfaces will electrostatically attract oppositely charged species (typically called counterions) in the solvent or solution. A combination of electrostatic forces, Brownian motion and osmotic forces would result in the formation of a so-called double layer structure, as schematically illustrated in Figure 1. The figure depicts a positively charged particle surface, the concentration profiles of negative ions (counterions) and positive ions (surface-charge-determining ions) and the electric potential profile. The concentration of counterions gradually decreases with distance from the particle surface, whereas that of charge-determining ions increases. As a result, the electric potential decreases with distance. Near to the particle surface, the electric potential decreases linearly, in the region known as the Stern layer. Outside the Stern layer, the decrease follows an exponential relationship, and the region between the Stern layer and the point where the electric potential equals zero is called the diffusion layer. Together, the Stern layer and diffusion layer are called the double layer structure in the classic theory of electrostatic stabilization.

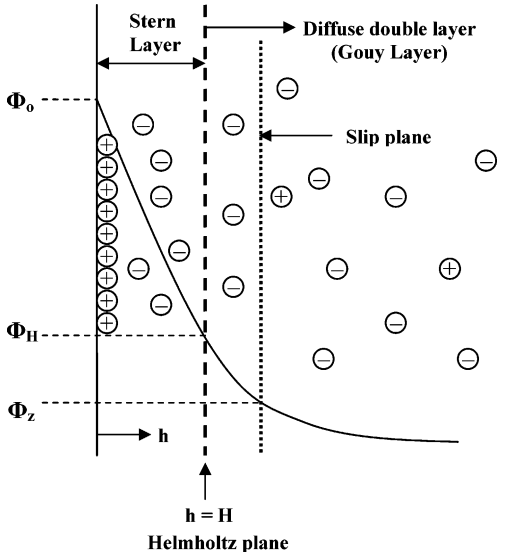

Figure 1. Schematic illustrating electrical double layer structure and the electric potential near the solid surface with both Stern and Gouy layers indicated. Surface charge is assumed to be positive.

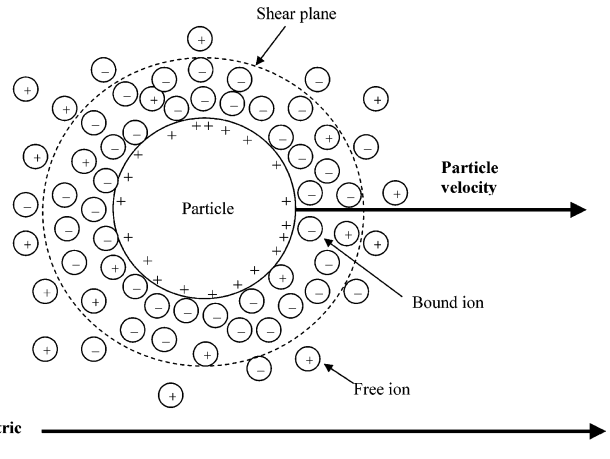

Figure 2. Schematic of electrophoresis of a charged particle in a colloidal suspension, demonstrating the motion in the direction of the applied electric field. Some of the solvent or solution surrounding the particle will move with it, since this part of the solvent or solution is tightly bound to the particle and separated from the rest solvent or solution by shear plane.

Upon application of an external electric field to a colloidal system or a sol, the constituent charged particles are set in motion in response to the electric field, as schematically illustrated in Figure 2. This type of motion is referred to as electrophoresis. When a charged particle is in motion, some of the solvent or solution surrounding the particle will move with it, since part of the solvent or solution is tightly bound to the particle. The plane that separates the tightly bound liquid layer from the rest of the liquid is called the slip plane. The electric potential at the slip plane is known as the zeta potential. The zeta potential is an important parameter in determining the stability of a colloidal dispersion or a sol; a zeta potential larger than about 25 mV is typically required to stabilize a system.[26] The zeta potential is determined by a number of factors, such

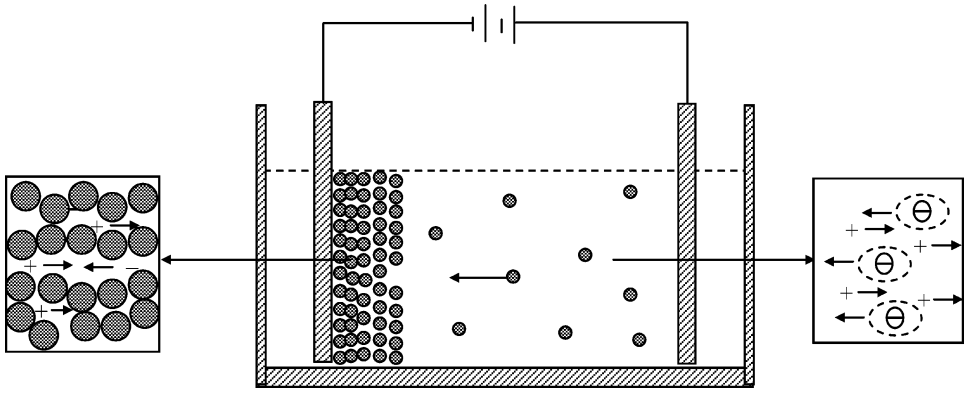

Figure 3. Schematic showing the electrophoretic deposition. Upon application of an external electric field to a colloidal system or a sol, the constituent charged nanoparticles or nanoclusters are set in motion in response to the electric field, whereas the counterions diffuse in the opposite direction.

as the particle surface charge density, the concentration of counterions in the solution, solvent polarity, and temperature. The zeta potential around a spherical particle can be described as[27]

$$\zeta = \frac{Q}{4\pi\epsilon_r a(1+\kappa a)} \tag{3}$$

with

$$\kappa = \left(\frac{e^2 \sum n_i z_i^2}{\epsilon_r \epsilon_0 kT}\right)^{(1/2)} \tag{4}$$

where Q is the charge on the particle, a is the radius of the particle out to the shear plane, ϵ_r is the relative dielectric constant of the medium, and n_i and z_i are the bulk concentration and valence of the ith ion in the system, respectively. It is worthwhile to note that a positively charged surface results in a positive zeta potential in a dilute system. A high concentration of counterions, however, can result in a zeta potential of the opposite sign.

The mobility of a nanoparticle, μ, in a colloidal dispersion or a sol is dependent on the dielectric constant of the liquid medium, ϵ_r, the zeta potential of the nanoparticle, ζ, and the viscosity of the fluid, η. Several forms for this relationship have been proposed, such as the Hückel equation[27]

$$\mu = \frac{2\epsilon_r \epsilon_0 \zeta}{3\pi\eta} \tag{5}$$

Double layer stabilization and electrophoresis are extensively studied subjects. Readers may find additional detailed information in books on sol−gel processing[18−20] and colloidal dispersions.[27−28]

Electrophoretic deposition simply uses such an oriented motion of charged particles to grow films or monoliths by enriching the solid particles from a colloidal dispersion or a sol onto the surface of an electrode as schematically illustrated in Figure 3. If particles are positively charged (more precisely speaking, having a positive zeta potential), then the deposition of solid particles will occur at the cathode. Otherwise, deposition will be at the anode. At the electrodes, surface electrochemical reactions proceed to generate or receive electrons. The electrostatic double layers collapse upon deposition on the growth surface, and the particles coagulate. There is not much information on the deposition behavior of particles at the growth surface. Some surface diffusion and relaxation is expected. Relatively strong attractive forces, including the formation of chemical bonds between two particles, develop once the particles coagulate. The films or monoliths grown by electrophoretic deposition from colloidal dispersions or sols are essentially a compaction of nanosized particles. Such films or monoliths are porous, i.e., there are voids inside. Typical packing densities, defined as the fraction of solid (also called green density) are less than 74%, which is the highest packing density for uniformly sized spherical particles.[29] The green density of films or monoliths by electrophoretic deposition is strongly dependent on the concentration of particles in sols or colloidal dispersions, zeta potential, externally applied electric field and reaction kinetics between particle surfaces. Slow reaction and slow arrival of nanoparticles onto the surface would allow sufficient particle relaxation on the deposition surface, so that a high packing density is expected.

Many theories have been proposed to explain the processes at the deposition surface during electrophoretic deposition. The electrochemical process at the deposition surface or electrodes is complex and varies from system to system. However, in general, a current exists during electrophoretic deposition, indicating that reduction and oxidation reactions occur at electrodes and/or the deposition surface. In many cases, films or monoliths grown by electrophoretic deposition are electric insulators. However, the films or monoliths are porous and the surface of the pores would be electrically charged just like the nanoparticle surfaces, since surface charge is dependent on the solid material and the solution. Furthermore, the pores are filled with solvent or a solution that contains counterions and charge-determining ions. The electrical conduction between the growth surface and the bottom electrode can proceed via either surface conduction or solution conduction. Since films or monoliths grown by electrophoretic deposition are porous, postdeposition sintering at elevated temperatures is usually required to form a dense material. However, considering the fact that the films or monoliths are a compaction of nanosized particles, sintering or densification is relatively easier than conventional ceramic sintering. If the initial solid particles were amorphous, sintering would also induce crystallization.

4. Growth of Oxide Nanorod Arrays by Sol Electrophoretic Deposition

A combination of sol preparation and electrophoretic deposition has been used to synthesize a variety of oxide nanorod arrays, such as TiO_2, SiO_2, Nb_2O_5, V_2O_5, $BaTiO_3$, Pb(Zr,Ti)-O_3, Sn-doped In_2O_3 (ITO), and $Sr_2Nb_2O_7$.[30−38] An overview of the chemicals and conditions for the preparation of the various sols is given in Table 1. Nanorod arrays of these oxides were

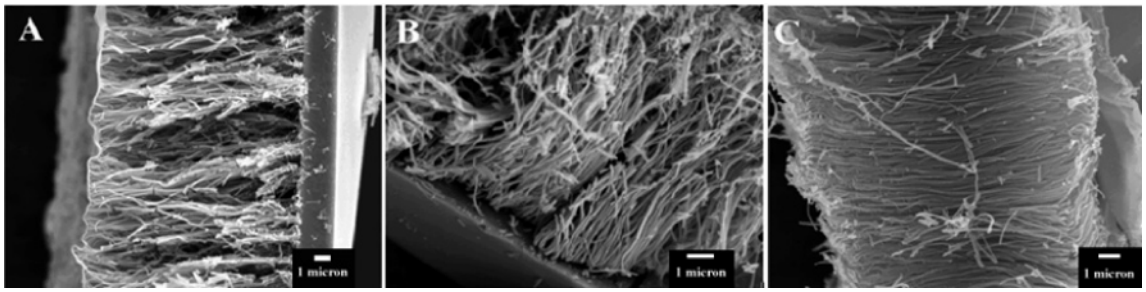

Figure 4. SEM micrographs of various TiO_2 nanorods. The length is ~10 μm, and the diameters are ~180 nm (A), ~90 nm (B), and ~45 nm (C). These correspond to about 10% lateral shrinkage from the original pore diameters. Samples were grown at 5 V for 90 min (A,B) or 60 min (C).

TABLE 1: Overview of the Chemicals and Conditions for the Preparation of the Various Sols for the Growth of Nanorod Arrays by Sol Electrophoretic Deposition

sol	precursors	solvents/other chemicals	approx pH
TiO_2	titanium (IV) isopropoxide	glacial acetic acid, water	~2
SiO_2	tetraethyl orthosilicate	ethanol, water, hydrochloric acid	~2
Nb_2O_5	niobium chloride	ethylene glycol, ethanol, citric acid, water	~1
V_2O_5	vanadium pentoxide	hydrogen peroxide, water, hydrochloric acid	~2.7
$Pb(Zr,Ti)O_3$	lead (II) acetate, titanium isopropoxide, zirconium *n*-propoxide	glacial acetic acid, water, lactic acid, glycerol, ethylene glycol	~4
$BaTiO_3$	titanium (IV) isopropoxide, barium acetate	glacial acetic acid, ethylene glycol	~4
$SrNb_2O_6$	strontium nitrate, niobium chloride	ethylene glycol, ethanol, citric acid, water	~1
ITO	indium chloride, tin (IV) chloride	ethylene glycol, ethanol, citric acid, water	~1

formed by the following method. Nanorod growth occurred on a working electrode of aluminum sheets or conductive carbon tapes, with a Pt mesh used as the counter electrode. The template membranes used for the growth of the nanorods were either track-etched hydrophilic polycarbonate with pore diameters of 50−200 nm and a thickness of 10 μm or anodic alumina membranes with pores of 200 nm and thickness of ~70 μm. The sol is drawn into the membrane pores by capillary action when the membrane is brought in contact with the sol. A Pt counter electrode is also placed in the sol, parallel to the working electrode. For most of the electrophoretic growth, a potential of 5 V is applied between the electrodes, and held for up to 60 min. At the end of the electrophoretic deposition, excess sol is blotted off the membrane. Samples prepared in this manner are dried at ~100 °C for several hours and then placed in an oven and fired for 15−60 min. The temperature for this firing is between 500 and 700 °C. This is to burn off the polycarbonate membranes, make the nanorods dense and crystallize the material (except crystalline V_2O_5 and amorphous SiO_2). Alumina membranes were removed by dissolving into 6 M NaOH for 60 min.

4.1. Simple Oxide Nanorod Arrays (TiO_2). In this section, TiO_2 nanorods will be used as a model system to illustrate the template-based growth by sol electrophoretic deposition. Figure 4 shows SEM micrographs of TiO_2 nanorods grown in polycarbonate membranes. Growth was in templates with 50−200 nm diameter pores, and 5 V was used for either 90 min (200 and 100 nm templates) or 60 min (50 nm template). All nanorods were fired at 500 °C for 60 min. These nanorods have a uniform diameter throughout their entire length, with a surface that is smooth over much or all of the length. Comparing the various rods, one can see that they all have roughly the same length and diameter. The image also shows that the rods arrange roughly parallel to one another over a broad area on the substrate. The diameter of the TiO_2 nanorods is estimated by measuring several tens of nanorods on each micrograph. The results of ~45−180 nm are approximately 10% smaller than the membrane pore diameter. This difference in size is most likely from the volume shrinkage caused by densification during the heat treatment. Upon heating nanorod samples to 700 °C, the shrinkage in diameter increases to about 25%. Thus, the nanorods are not fully dense after heating to only 500 °C for 60 min; however, it is necessary to use a lower temperature if one wishes to have the anatase phase. Figure 4 also shows some broken rods, and it can be seen that these rods are solid and dense. Furthermore, Figure 4A shows that a thick layer was formed at one end of the nanorods (right-hand side), where the template contacted the sol during deposition. This sample was grown for a longer time, implying that the growth of the nanorods likely begins at the bottom of the pores and proceeds from one side of the membrane to the other. For the TiO_2 rods grown in 50 nm templates, the drying time used exerts a strong influence on the fidelity of the nanorods. Samples dried at 100 °C for up to 24 h showed no nanorods after firing at 500 °C. In samples dried for ~48 h prior to firing, however, nanorods were observed. It is likely that this result is due to the increased degree of condensation that occurred in the sample dried for a longer time. By allowing the samples to undergo further condensation reactions, the rods formed were likely stronger and thus better able to resist breakage upon firing.

It is common that the oxide nanorods, grown in polycarbonate membrane by electrophoretic deposition with the membrane removed by pyrolysis at elevated temperatures, are distorted or broken instead of being straight and intact. Such distortion or breakage is due to the weak mechanical strength of the initial nanorods that are simply made by stacking nanoclusters together; only van der Waals force and limited chemical bonds (through surface condensation) are present to hold nanoclusters together. When the polycarbonate membrane is heated to an elevated temperature, it undergoes relatively large thermal expansion and warping. When oxide nanorods were grown in anodic alumina membranes, nanorods showed much improved morphology (better alignment and more straight) as shown in Figure 5.

Figure 6A shows a TEM micrograph of a TiO_2 nanorod grown in a 200 nm PC template at 1.67 V/cm for 30 min. The micrograph demonstrates that the nanorods are quite smooth and dense. Figure 6B shows a high-resolution TEM image and electron diffraction pattern, demonstrating that the nanorods are polycrystalline, with grains that are ~5 nm in size. This value is larger than the estimated size of the nanoparticles in the TiO_2

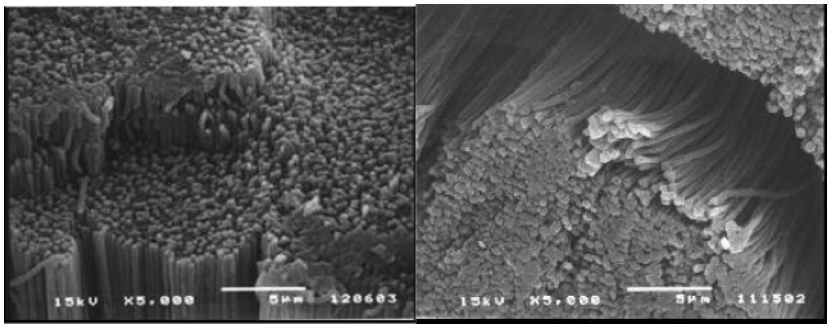

Figure 5. SEM images of TiO_2 nanorods grown in anodic alumina membrane, which was subsequently removed by solving into 6M NaOH solution.

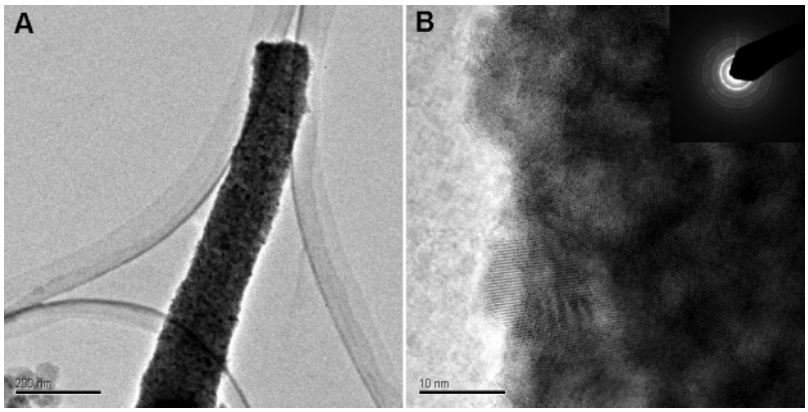

Figure 6. TEM micrographs of a TiO_2 nanorod grown in a 200 nm PC template at 1.67 V/cm for 30 min. Part A shows a single nanorod, demonstrating that the nanorods are quite smooth and dense. Part B shows a high-resolution TEM image and electron diffraction pattern, demonstrating that the nanorods are polycrystalline, with grains of ~5 nm in size.

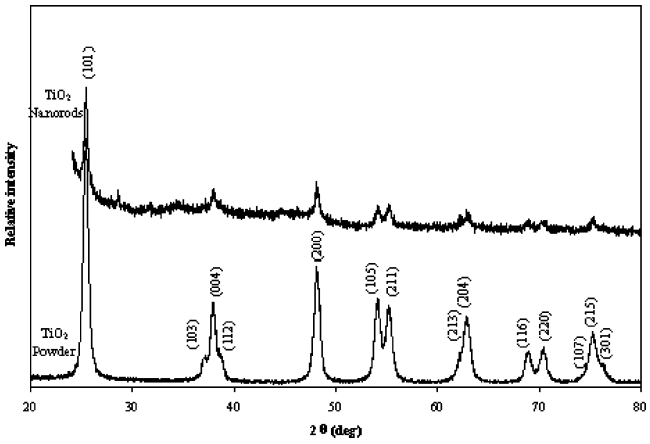

Figure 7. XRD spectra of both the grown TiO_2 nanorods and a powder derived from the same sol. Both samples consist the anatase phase, and there is no observed shift in the peak positions for the nanorod sample. In addition, the relative intensities of the peaks are the same for the nanorod sample, showing that there is no preferred orientation in the sample.

sol (~1 nm); however, the TiO_2 nanorod shown in this micrograph was fired at 700 °C, which would likely lead to larger grains. XRD spectra of the TiO_2 rods are shown in Figure 7, along with the spectra for a powder formed from the same sol and fired at 500 °C for 60 min. From the powder XRD spectrum, it can be seen that the sample consists of the anatase phase. Note that there is a large amorphous background associated with the TiO_2 nanorods. This is owing to the small volume of nanorods available for analysis, meaning that much of the X-ray beam was hitting the (amorphous) sample holder. Higher sintering temperatures should lead to the formation of entirely rutile TiO_2 nanorods, although anatase has been found to be stable up to 800 °C in acetic acid-modified TiO_2 systems.[39]

4.2. Complex Oxide Nanorod Arrays (PZT). Figure 8 shows SEM images of the PZT nanorods grown from the PZT sol by means of electrophoretic deposition and fired at 700 °C for 60 min in air. PZT nanorods grown in PC membranes with pore sizes of 50−200 nm show uniform size and near-unidirectional alignment. The PZT nanorods grown in both the 100 and 200 nm membranes show a uniform diameter throughout the entire length (Figure 8, parts A and B), with a surface that is smooth over much or all of the length, where those grown in the 50 nm templates are less straight and parallel (Figure 8C). The PZT nanorods have diameters smaller than that of the pores in the template membranes, estimated by measuring several tens of nanorods on each micrograph. The PZT nanorods have a size of approximately 45 nm when grown in a PC membrane with pores of 50 nm, 70 nm when grown in a 100 nm template, and 150 nm when grown in a membrane with 200 nm pores. The diameter difference of the grown nanorods and pores in the membranes could be attributed to the densification of nanorods when fired at 700 °C. However, it is not known why the samples grown in different templates show much different shrinkage, with about 25−30% shrinkage seen in the 100 and 200 nm templates and about 10% shrinkage in the 50 nm templates. The 100 and 200 nm samples shown were grown in the original experimental setup, whereas the 50 nm sample was grown in the revised setup, and thus, the high resistance of the carbon tape working electrode may account for the lower deposit density in the earlier samples.

Figure 9 shows XRD spectra of the PZT nanorods and PZT powder prepared from the same sol by drying overnight at ~110 °C and firing at 700 °C for 1 h; both PZT nanorods and powder consisted of only one crystalline phase, perovskite PZT without

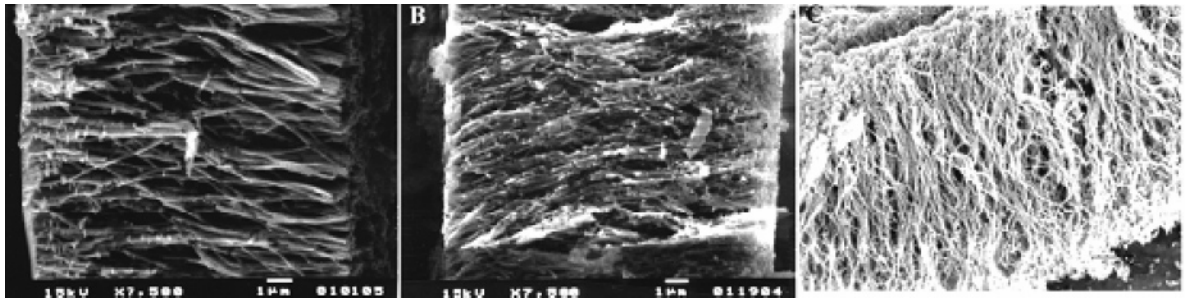

Figure 8. SEM micrographs of PZT nanorods. The lengths are ~10 μm and the diameters are ~150 nm (A), ~70 nm (B), and ~45 nm (C).

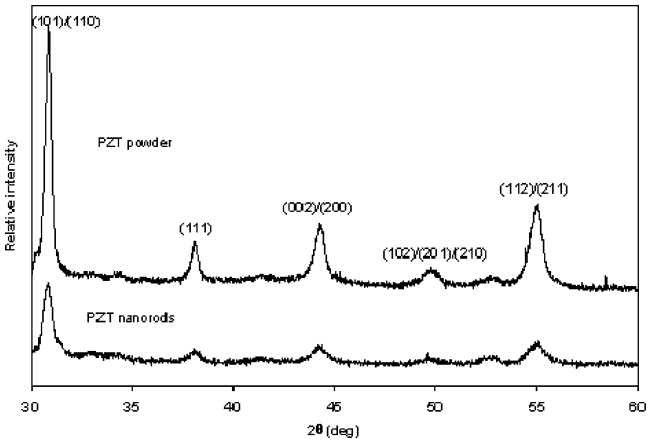

Figure 9. XRD spectra of both the grown PZT nanorods and a powder derived from the same sol. Both samples show only a single perovskite phase. This demonstrates that sol−gel electrophoresis can be used to form complex oxides with the desired stoichiometry and crystal phase.

any detectable secondary phase. Comparison of the two spectra shows that there are identical peaks in both samples. Further, the peak positions are the same and the intensity ratios among various peaks are identical. The above XRD results indicate that the electrophoretic deposition has no detrimental influence on the stoichiometry and chemical compositional homogeneity that is achieved during the sol preparation.[40] Furthermore, there is no preferred orientation of the crystals in the PZT nanorods.

4.3. Doped Oxide Nanorod Arrays (ITO). Figure 10 shows SEM micrographs of ITO nanorods grown in 100 (A) and 200 (B) nm PC templates at 1.33 V/cm for 60 min, and fired at 600 °C for 1 h. These samples show about 25−30% shrinkage in diameter compared to the original template diameter. The nanorods synthesized in this study are not straight, with a number of the nanorods exhibiting noticeable curvature. One possible explanation for this is the length of the drying step used prior to firing. It is believed that this step promotes further surface condensation reactions between the deposited nanoparticles and is thus an important part of the nanorod synthesis. This can be seen, for example, in the growth of TiO_2 nanorods in 50 nm templates, where the morphology changes between samples dried for ~24 (discontinuous) and ~48 h (continuous) at 110 °C.[33] It is thus possible that a further drying time (or increase in drying temperature) could further the surface condensation, and thus yield straighter rods. To understand the importance of EPD on the growth of the ITO nanorods, samples were also prepared without electrophoresis, by simply immersing the 200 nm PC template into the sol for 1 h. Figure 10C shows an SEM micrograph of such a sample. It can be seen in this image that the result of the growth without EPD is a low yield of short, broken, and hollow nanorods. This is expected, given the expected mechanism of growth when using sol EPD. Figure 11 shows XRD spectra of ITO powder and ITO nanorods in an AAM template, prepared from the same sol. Both nanorods and powder comprise one crystalline phase, cubic In_2O_3. There is, however, a peak in the nanorod sample that does not belong to ITO, or any tin or indium oxides, but may be from the alumina template. Comparison of the two spectra shows that there are identical peaks in both samples. Similar to PZT, these XRD results indicate that the electrophoretic deposition has no detrimental influence on the stoichiometry and chemical compositional homogeneity that is achieved during the sol preparation.

Figure 12A shows a bright-field TEM micrograph of a single ITO nanorod grown in 100 nm PC template at 1.33 V/cm for 1 h. From this image, one can see that the nanorod has a mostly smooth surface but that there are some small fluctuations on the sides of the rod. The selected area diffraction pattern (Figure 12B) of one nanorod shows a ring pattern typical of a polycrystalline nanorod. A dark-field TEM image (Figure 12C) shows the presence of very small crystallites, ~2−5 nm in size. This is somewhat smaller than the grain sizes determined from XRD line broadening, which show an average crystallite size of ~25 nm in the nanorods. This is not surprising, as ITO has been found with a "grain sub-grain structure", where the smaller subgrains are about twenty times smaller than the grains.[41] XRD line broadening is also of limited accuracy for very fine-grained

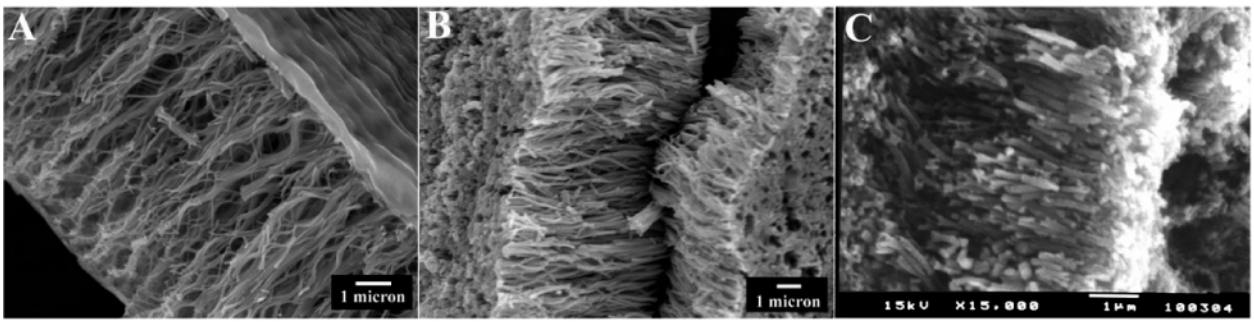

Figure 10. Parts A and B showing SEM micrographs of nanorods of ITO grown in 100 nm (A) and 200 nm (B) templates at 1.33 V/cm for 60 min. Part C is an SEM micrograph of a sample where EPD was not used, showing poor quality nanorods.

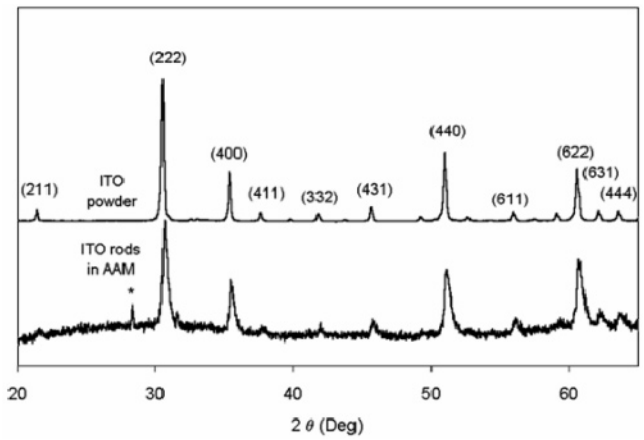

Figure 11. XRD patterns for ITO powders and nanorods (in AAM) fired in air at 700 °C for 1 h. The peak marked * does not belong to ITO, or any tin or indium oxides, but may be from the alumina template.

compacts due to the presence of nonuniform strains.[42] Figure 12D shows the recorded EDS data from a single nanorod. Both the In (24.14 keV) and Sn (25.20 keV) K_α lines[43] are clearly present, with an intensity ratio that suggests ~8% Sn in the In_2O_3. Sn is present in the nanorods, showing that we have successfully produced the desired, doped phase of ITO.

4.4. Single-Crystal Oxide Nanorod Arrays by Sol Electrophoretic Deposition. Single crystalline oxide nanorod arrays can also been grown by template-based sol electrophoretic deposition, provided that crystalline nanoclusters are formed during sol preparation. Figure 13 (left) shows typical TEM micrographs and selected-area electron diffraction patterns of V_2O_5 nanorods, and the diffraction patterns clearly proved the single-crystalline or, at least, well oriented nature of the nanorods. All of the diffraction patterns can be indexed as orthorhombic V_2O_5 on a [001] zone axis. When the image of the nanorod is overlaid on the diffraction pattern, one observes that the long axis of the nanorod points toward the (020) spot. Thus, if growth occurs along the length of the nanorod, then this information suggests a [010] growth direction for the nanorods. Figure 13 (right) is the high-resolution TEM micrograph of a single V_2O_5 nanorod, in which lattice fringes are clearly visible. The spacing of the fringes was measured to be 0.208 nm. This value corresponds well with the spacing of (202) planes at 0.204 nm. These fringes make an angle of 88.9° with the long axis of the nanorod, which is consistent with a growth direction of [010]. Similar measurements made on high-resolution images of other nanorods also yield results consistent with a [010] growth direction.

The formation of single crystalline vanadium pentoxide nanorods by template-based sol electrophoretic deposition can be attributed to homoepitaxial aggregation of crystalline nanoparticles. Thermodynamically it is favorable for the crystalline nanoparticles to aggregate epitaxially; such growth behavior and mechanism have been well documented in literature.[44,45] In this growth mechanism, the initial weak interaction between two nanoparticles allows rotation and migration relative to each other. Obviously, homoepitaxial aggregation is a competitive process and porous structure is expected to form through such homoepitaxial aggregation (as schematically illustrated in Figure 14). Vanadium oxide particles in a typical sol are known to form an ordered crystalline structure easily,[46] so that it is reasonable to expect that homoepitaxial aggregation of vanadia nanocrystals from sol results in the formation of single crystal nanorods. Such formed single crystal nanorods are likely to undergo significant shrinkage when fired at high temperatures due to its original porous nature; 50% lateral shrinkage has been observed in vanadium pentoxide nanorods formed by this method. In addition, it might be possible that the electric field

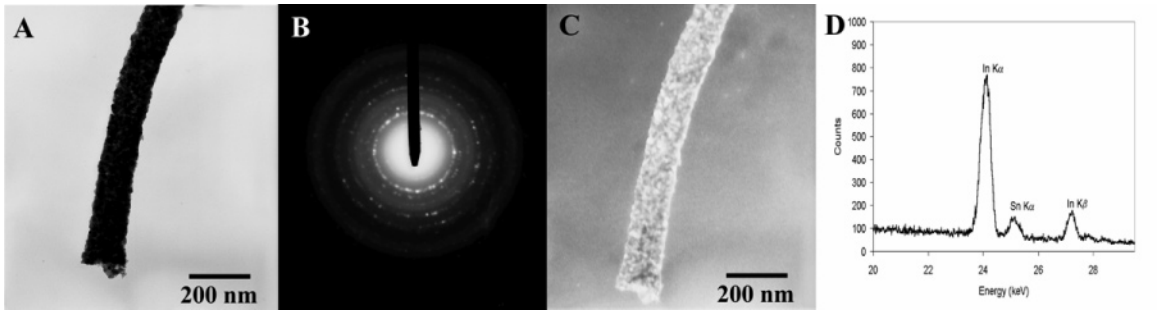

Figure 12. Single ITO nanorod grown in a 100 nm PC template at 1.33 V/cm for 1 h. Part A shows a bright-field TEM micrograph. Part B is an electron diffraction pattern from that rod. Part C is a dark-field TEM micrograph, demonstrating the small crystallite size. Part D shows the EDS spectrum of a single ITO nanorod.

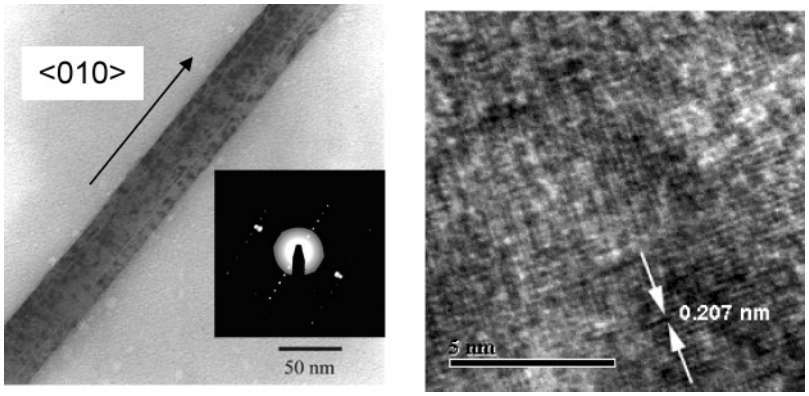

Figure 13. Typical TEM micrograph and selected-area electron diffraction pattern of vanadium pentoxide nanorods (left) and the high-resolution TEM image showing lattice fringes.

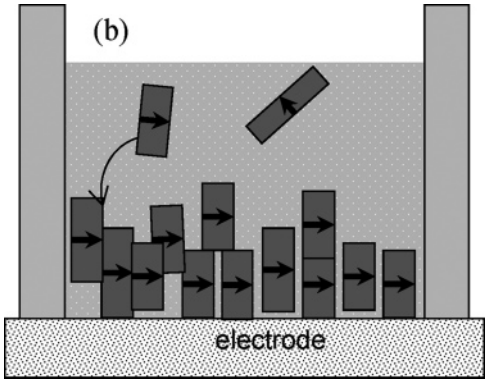

Figure 14. Schematic showing the growth of a single-crystal nanorod inside a template pore channel through homoepitaxial aggregation of crystalline nanoclusters.

and the internal surface of pore channels both play a significant role in the orientation of nanorods, as suggested in the literature.[47,48]

4.5. Single-Crystal Oxide Nanorod Arrays by Surface Condensation. A modified version of sol electrophoretic deposition has been demonstrated to be capable of growing single crystalline vanadium pentoxide nanorod arrays from VO_2^+ solution. In a typical sol−gel processing, nanoclusters are formed through homogeneous nucleation and subsequent growth through sequential yet parallel hydrolysis and condensation reactions. Sol electrophoretic deposition is to enrich and deposit such formed nanoclusters at an appropriate electrode surface under an external electric field. The modified process is to limit and induce the condensation reaction at the growth surface through the change of local pH value, which is a result of partial water hydrolysis at the electrode or growth surface

$$2H_2O + 2e^- \rightarrow H_2 + 2OH^- \quad (6)$$

$$2VO_2^+ + 2\,OH^- \rightarrow V_2O_5 + H_2O \quad (7)$$

Reaction 6, or the electrolysis of water, plays a very important role here. As the reaction proceeds, hydroxyl groups are produced, resulting in an increased pH at the proximity of the deposition surface. Such an increase of pH value near to the growth surface initiated and promoted the precipitation of V_2O_5, or reaction 7. The initial pH of the VO_2^+ solution is approximately 1.0, in which VO_2^+ is stable. However, when pH increases to ~1.8, VO_2^+ is no longer stable and solid V_2O_5 would form. Since the change of pH occurs at the proximity of the growth surface, reaction 7 or deposition is likely to occur on the surface of the electrode through heterogeneous nucleation and subsequent growth. It should be noted that the hydrolysis of water has another influence on the deposition of solid V_2O_5. Reaction 3 produces hydrogen on the growth surface. Such molecules may poison the growth surface before dissolving into the electrolyte or forming a gas bubble, which may cause the formation of porous nanorods.

The formation of single crystal nanorods from solutions by pH change induced surface condensation has been proven by TEM analyses including a high resolution image showing the lattice fringes and electron diffraction. The growth of single crystal nanorods by pH change induced surface condensation is attributed to evolution selection growth, which is briefly summarized below. The initial heterogeneous nucleation or deposition on the substrate surface results in the formation of nuclei with random orientation. The subsequent growth of various facets of a nucleus is dependent on the surface energy and varies significantly from one facet to another.[49] For one-dimensional growth, such as film growth, only the highest growth rate with a direction perpendicular to the growth surface will be able to continue to grow. The nuclei with the fastest growth direction perpendicular to the growth surface will grow larger, whereas nuclei with slower growth rates will eventually cease to grow. Such a growth mechanism would result in the formation of columnar structured films with all of the grains having the same crystal orientation (known as textured films).[50,51] In the case of nanorod growth inside a pore channel, such evolution selection growth is likely to lead to the formation of a single-crystal nanorod or a bundle of single-crystal nanorods per pore channel (Figure 15). It is well-known that [010] or the *b* axis is the fastest growth direction for the V_2O_5 crystal,[52,53] which would explain why single-crystal vanadia nanorods or a bundle of single-crystal nanorods grow along the *b* axis. Single crystalline TiO_2 nanowires were also grown using this method by Miao et al.[54]

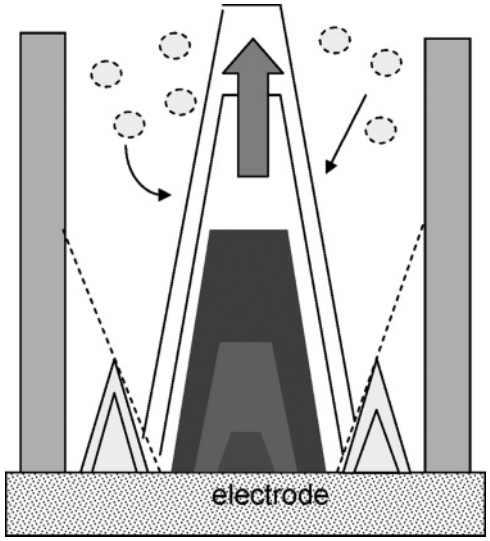

Figure 15. Schematic showing the mechanism of evolution selection growth inside a pore channel leading to the formation of single-crystal nanorod.

4.6. Metal-Oxide Core−Shell Nanocable Arrays. Figure 16 shows the SEM micrographs of Ni nanorod arrays and Ni−V_2O_5 core−shell nanocable arrays.[55] Ni nanorod arrays were grown in PC membrane by electrochemical deposition from nickel sulfate solution. After the removal of the PC membrane by dissolving in ethylene chloride, a vanadium pentoxide coating was deposited onto the surface of Ni nanorods by sol electrophoretic deposition. Figure 17 demonstrated that a thin vanadium pentoxide layer of approximately 30 nm in thickness was deposited on the surface of the Ni nanorod with uniform confirmal coverage. Such an electrical conductive core and dielectric shell nanocable structure can be made by a combination of electrochemical deposition and sol electrophoretic deposition.

5. Properties and Applications of Oxide Nanorod Arrays

All oxide nanorod arrays grown by sol electrophoretic deposition are expected to have physical properties similar to that of sol−gel films, since, in most cases, oxide nanorods are polycrystalline and consist of particles similar to those in sol−gel films, when formation and subsequent processing conditions, such as annealing temperature and duration time, are kept the same. Although particles are found to be several to several tens of nanometers in size, no quantum confinement or unexpected

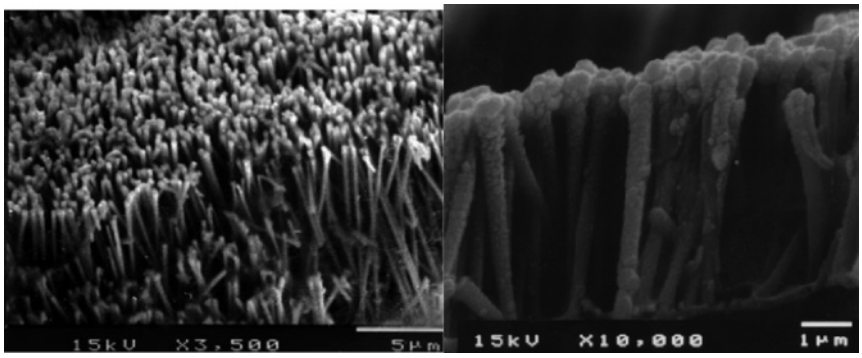

Figure 16. SEM micrographs of Ni nanorod arrays (left) and Ni − V_2O_5 core−shell nanocable arrays (right).

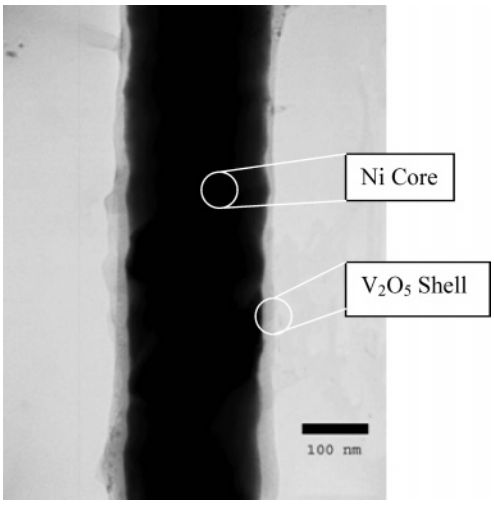

Figure 17. TEM micrographs of a Ni−V_2O_5 core−shell nanocable showing ~30 nm vanadium pentoxide (shell) coated on Ni nanowire (core).

properties have been found in our study so far. The only exception is the increase of Curie temperature in PZT nanorod arrays.[56]

Despite the similar physical properties found in oxide nanorod arrays as that of bulk form, they do offer various advantages when integrated into devices or systems for practical applications, due largely to their large surface area and enhanced transport properties, particularly when the nanorods are of single crystal. For example, single crystalline vanadium pentoxide nanorod arrays have demonstrated significantly improved electrochemical properties with both lithium intercalation capacity and intercalation and an extraction rate of 5 times better than that of sol−gel derived films.[36,38] Such vanadia nanorod arrays would offer significantly enhanced performance when used in electrochemical pseudocapacitors and electrochromic displays. Another example is the freedom that nanorod arrays possess, which offer a relatively easy change of dimensions in lateral directions. In the case of intercalation of lithium in layer structured vanadium pentoxide nanorod arrays, such a freedom of easy change of lateral dimensions means not only easy intercalation process, but also an improved cyclic fatigue resistance and thus a prolonged lifetime. Such lateral freedom would also permit piezoelectric nanorod arrays to generate greater strain as compared to its bulk counterpart. Uniformly sized and unidirectional aligned oxide nanorod arrays over a large area permits direct fabrication of macroscopic devices. The ability to grow various oxide nanorod arrays, particularly, complex oxide nanorod arrays, makes it possible to explore various functional properties of various oxides in nanostructured devices and systems.

6. Concluding Remarks

Sol electrophoretic deposition is a simple combination of sol preparation and electrophoretic deposition. When combined with template-controlled growth, unidirectionally aligned and uniformly sized nanorod arrays over a large area can be readily formed. When the sol−gel process is appropriately controlled, a variety of complex oxide and doped-oxide nanorod arrays can be grown by this simple method. Although it has not been demonstrated experimentally, the growth of organic−inorganic hybrid nanorod arrays would be possible since it is similar to that of complex oxide nanorod arrays. For the growth of complex oxide and organic−inorganic hybrid nanorods, it is critical to ensure hetero-condensation among various precursors so that homogeneous composition can be obtained. If homogeneous condensation reactions are predominant, nanoclusters with different chemical composition, size, and shape may form and lead to the formation of composition graded nanorods, which can be explored for the growth of nanorod arrays of

TABLE 2: Brief Summary of Advantages and Limitations of Sol Electrophoretic Deposition for the Growth of Nanorod Arrays

advantages and limitations	comments
uniform size, easily controlled by selection of template	
unidirectional alignment	unlike many nontemplate solution methods, where the nanorods are randomly dispersed in a solvent
large area arrays possible	only limited by the size of membranes and electrodes
simple and inexpensive experimental setup	only requires supplies found in many labs, no specialized equipment
simple and complex oxides	few other techniques offer a general synthesis of all oxide materials
require sintering to make dense and crystallize	
distortion of nanorods and reactions with template	nanorods may deform upon removal of template and nanorods may react with template
polycrystalline	while not a disadvantage for all applications, in some situations single-crystal nanorods would be preferred
possible microstructure gradients	may be advantageous for making functionally graded materials
must control chemistry to obtain desired product	for complex oxides and organic−inorganic hybrids, homo-condensation must be avoided

functionally graded materials. Although sol electrophoretic deposition primarily results in the formation of polycrystalline oxide nanorod arrays, it has been demonstrated that single crystalline oxide nanorod arrays can be grown through either homoepitaxial aggregation or surface condensation induced by water hydrolysis. Table 2 gives a brief summary of major advantages and limitations of sol electrophoretic deposition.

Acknowledgment. Most of the results presented in this paper are from Dr. Steven J. Limmer's PhD dissertation. Other results are from the research work of Katsunori Takahashi and Tammy P. Chou. This work has been supported by the Center for Nanotechnology at UW, Pacific Northwest National Laboratories (PNNL), Joint Institute of Nanoscience and Nanotechnology (JIN, UW and PNNL), Washington Technology Center (WTC), and JFE Steel Corporation in Japan. Dr. Limmer's work was supported by NSF-IGERT, Ford, Nanotechnology, and JIN graduate fellowships, and Chou's work was supported by JIN and Intel PhD graduate fellowships, and JFE Steel Corporation supported Takahashi's research. A portion of the research (TEM study) described in this paper was performed in the Environmental Molecular Sciences Laboratory, a national scientific user facility sponsored by the Department of Energy's Office of Biological and Environmental Research and located at PNNL.

References and Notes

(1) Moulson, A. J.; Herbert, J. M. *Electroceramics: Materials, Properties, Applications*; Chapman and Hall: London, 1990.
(2) Kholkin, A. *Ferroelectrics* **2001**, *258*, 209.
(3) Tak, Y.-H.; Kim, K.-B.; Park, H.-G.; Lee, K.-H.; Lee, J.-R. *Thin Solid Films* **2002**, *411*, 12.
(4) Conway, B. E. *Electrochemical Supercapacitors*; Plenum Publishing: New York, 1999.
(5) Stathatos, E.; Lianos, P.; Lavrencic-Stangar, U.; Orel, B. *Adv. Mater.* **2002**, *14*, 354.
(6) Wu, Y.; Forbess, M. J.; Seraji, S.; Limmer, S. J.; Chou, T. P.; Nguyen, C.; Cao, G. Z. *J. Appl. Phys.* **2001**, *90*, 5296.
(7) Richerson, D. W. *Modern Ceramic Engineering*; Marcel Dekker: New York, 1992.
(8) Peña, M. A.; Fierro, J. L. G. *Chem. Rev.* **2001**, *101*, 1981.
(9) Impens, N. R. E. N.; van der Voort, P.; Vansant, E. F. *Micropor. Mesopor. Mater.* **1999**, *28*, 217.
(10) Cao, G. Z. *Nanostructures and Nanomaterials: Synthesis, Properties, and Applications*; Imperial College Press: London, 2004.
(11) Pan, Z. W.; Dai, Z. R.; Wang, Z. L. *Science* **2001**, *291*, 1947.
(12) Li, Y.; Cheng, G. S.; Zhang, L. D. *J. Mater. Res.* **2000**, *15*, 2305.
(13) Pan, Z. W.; Dai, Z. R.; Ma, C.; Wang, Z. L. *J. Am. Chem. Soc.* **2002**, *124*, 1817.
(14) Liu, J.; Lin, Y.; Liang, L.; Voigt, J. A.; Huber, D. L.; Tian, Z. R., Coker, E.; Mckenzie, B.; Mcdermott, M. J. *Chem.: Eur. J.* **2003**, *97*, 604.
(15) Tian, Z. R.; Voigt, J. A.; Liu, J.; Mckenzie, B.; Mcdermott, M. J.; Cygan, R. T.; Criscenti, L. J. *Nat. Mater.* **2003**, *2*, 821.
(16) Lakshmi, B. B.; Patrissi, C. J.; Martin, C. M. *Chem. Mater.* **1997**, *9*, 2544.
(17) Cheng, B.; Samulski, E. T. *J. Mater. Chem.* **2001**, *11*, 2901.
(18) Brinker, C. J.; Scherer, G. W. *Sol−Gel Science: The Physics and Chemistry of Sol−Gel Processing*; Academic Press: Boston, 1990.
(19) Pierre, A. C. *Introduction to Sol−Gel Processing*; Kluwer Academic Publishers: Boston, 1998.
(20) Wright, J. D.; Sommerdijk, N. A. J. M. *Sol−Gel Materials: Chemistry and Applications*; Gordon and Breach Science Publishers: Amsterdam,
2001.
(21) Matsuda, H.; Kobayashi, N.; Kobayashi, T.; Miyazawa, K.; Kuwabara, M. *J Non-Cryst. Solids* **2000**, *271*, 162.
(22) Haruta, M.; Delmon, B. *J. Chim. Phys.* **1986**, *83*, 859.
(23) Nielsen, A. E. *Kinetic of Precipitation*; MacMillan: New York, 1964.
(24) Stein, A.; Schroden, R. C. *Curr. Opin. Solid State Mater. Sci.* **2001**, *5*, 553.
(25) Oldenburg, S. J.; Averitt, R. D.; Westcott, S. L.; Halas, N. J. *Chem. Phys. Lett.* **1998**, *288*, 243.
(26) Reed, J. S. *Introduction to the Principles of Ceramic Processing*; John Wiley & Sons: New York, 1988.
(27) Hunter, R. J. *Zeta Potential in Colloid Science: Principles and Applications*; Academic Press: London, 1981.
(28) Everett, D. H. *Basic Principles of Colloid Science*; Royal Society of Chemistry: London, 1988.
(29) Callister, W. D. *Materials Science and Engineering: An Introduction*; John Wiley & Sons: New York, 1997.
(30) Limmer, S. J.; Seraji, S.; Forbess, M. J.; Wu, Y.; Chou, T. P.; Nguyen, C.; Cao, G. Z. *Adv. Mater.* **2001**, *13*, 1269.
(31) Limmer, S. J.; Seraji, S.; Wu, Y.; Chou, T. P.; Nguyen, C.; Cao, G. Z. *Adv. Funct. Mater.* **2002**, *12*, 59.
(32) Limmer, S. J.; Hubler, T. L.; Cao, G. Z. *J. Sol−Gel Sci. Technol.* **2003**, *26*, 577.
(33) Limmer, S. J.; Cao, G. Z. *Adv. Mater.* **2003**, *15*, 427.
(34) Limmer, S. J.; Chou, T. P.; Cao, G. Z. *J. Mater. Sci.* **2004**, *39*, 895.
(35) Limmer, S. J.; Vince Cruz, S.; Cao, G. Z. *Appl. Phys.* **2004**, *A79*, 421.
(36) Takahashi, K.; Limmer, S. J.; Wang, Y.; Cao, G. Z. *J. Phys. Chem. B* **2004**, *108*, 9795.
(37) Limmer, S. J.; Chou, T. P.; Cao, G. Z. *J. Mater. Res.*, unpublished results.
(38) Takahashi, K.; Limmer, S. J.; Wang, Y.; Cao, G. Z. *Jpn. J. Appl. Phys.*, in press.
(39) Kumar, S. R.; Suresh, C.; Vasudevan, A. K.; Perumal, P.; Warrier, K. G. K. *Trans. 1nd. Ceram. Soc.* **1999**, *58*, 118.
(40) In the preparation of PZT sol, an excess amount of 5 mol % lead was added to compensate for the possible loss of PbO during sintering due to its volatility. Any excess amount of lead oxide that remains after sintering will form grain boundary phase. The Zr/Ti ratio can be precisely controlled by the initial concentrations of the respective precursors added and no loss of either titanium or zirconium is expected during the subsequent sintering process. The composition of the PZT crystal grains is $PbZr_{0.48}Ti_{0.52}O_3$.
(41) Kamei, M.; Shigesato, Y.; Takaki, S. *Thin Solid Films* **1995**, *259*, 38.
(42) Cullity, B. D. *Elements of X-ray Diffraction*, 2nd ed.; Addison-Wesley: Reading, MA, 1978.
(43) Feldman, L. C.; Mayer, J. W. *Fundamentals of Surface and Thin Film Analysis*; Elsevier Science Publishing Co., Inc.: New York, 1986.
(44) Penn, R. L.; Banfield, J. F. *Geochim. Cosmochim. Acta* **1999**, *63*, 1549.
(45) Chun, C. M.; Navrotsky, A.; Aksay, I. A. *Proc. Microsc. Microanal.* **1995**, 188.
(46) Livage, J. *Coord. Chem. Rev.* **1998**, *999*, 178−180.
(47) Saban, K. V.; Thomas, J.; Varughese, P. A.; Varghese, G. *Cryst. Res. Technol.* **2002**, *37*, 1188.
(48) Grier, D.; Ben-Jacob, E.; Clarke, R.; Sander, L. M. *Phys. Rev. Lett.* **1986**, *56*, 1264.
(49) van der Drift, A. *Philips Res. Rep.* **1968**, *22*, 267.
(50) Cao, G. Z.; Schermer, J. J.; van Enckevort, W. J. P.; Elst, W. A. L. M.; Giling, L. J. *J. Appl. Phys.* **1996**, *79*, 1357.
(51) Ohring, M. *Materials Science of Thin Films*; Academic Press: San Diego, CA, 2001.
(52) Pan, D.; Shuyuan, Z.; Chen, Y.; Hou, J. G. *J. Mater. Res.* **2002**, *17*, 1981.
(53) Petkov, V.; Trikalitis, P. N.; Bozin, E. S.; Billinge, S. J. L.; Vogt, T.; Kanatzidis, M. G. *J. Am. Chem. Soc.* **2002**, *124*, 10157.
(54) Miao, Z.; Xu, D.; Ouyang, J.; Guo, G.; Zhao, Z.; Tang, Y. *Nano Lett.* **2002**, *2*, 717.
(55) Takahashi, K.; Wang, Y.; Cao, G. Z. *Adv. Mater.*, unpublished results.
(56) Wang, Y.; Limmer, S. J.; Cao, G. Z. unpublished results.